Military Technical College
Kobry El-Kobbah
Cairo, Egypt

10th International Conference
On Aerospace Sciences&
Aviation Technology

The simulation of the occurance of a sand storm using the Egyptian numerical model

Kamal F. and A. Yousef
Egyptian Meteorological Authority

Abstract

Among different weather phenomena that occur in subtropical Africa, one stands out as being most unpleasent for the population of this area, most hazardous for transport and navigation are duststorms. These storms are frequently invading the area by more than 20-25 storms / year. As these storms are small-scale phenomena, there is some difficulty in its analysis and forecasting. Usually these storms bring up more than 1350 $\mu g/m^3$ of sand load near the earth surface.

In present work, a dust model was under developing at Cairo numerical weather prediction NWP center to forecast and monitoring the dust and sandstorm. An equation for sand concentration was added to the hydrostatic primitive Egypt-eta model (Yousef. 98). The model depends on the soluation of a set of primitive equations using the generalized vertical coordinate, which follow the orographic structure. A forward – backward time integration scheme, as economic scheme, was used with the part control the fast waves to increase the time step. Forward –centered time integration scheme was used with the advection terms. A semi- Lagrangian advection scheme with fourth order accuracy has been modified to conserve the mass of dust. It uses full physical parameterization package as a detail representation of radiation components, surface physics-soil hydrology processes and comprehensive scheme for the planetary boundary layer has been used. In addition, eight levels in the boundary layer have been used to improve the forecasting of the surface temperature and capture well process occurring in the planetary boundary layer.
The dust module includes dust emission as a function of (vegetation cover- soil type and texture – soil wetness – friction velocity), dust deposition (wet and dry), horizontal and vertical advection and vertical diffusion through an improved formulation of planetary boundary layer.

Two cases with very remarkable sandstorms were described and investigated through this study. The model outputs for 72 hours were validated and verified with satellite images and visibility as actual data in addition, the aerodynamical parameters (friction velocity, wind speed, vertical motion) for the sake of comparison which are the main factors in the dust emission.

Introduction:

Recently, the first phase of the developing of a regional modeling system (Egypt-ETA) has been completed at Cairo center for NWP. It is based on the hydrostatic primitive equations using the generalized vertical coordinate, which follow the orographic structure Simmons, A.J. and Burridge [12]. The hybrid coordinate system combines the advantage terrain following sigma coordinate system near the surface, and the pressure system in the medium and upper troposphere and stratosphere, thereby reducing the error in the pressure gradient term. In the same time the numerical solutions are controlled by conservation of integral properties of the continuous equations. A split-explicit time differencing scheme Gadd [5] has been used to save computation time. A semi-staggered horizontal E-grid combined with a technique for preventing separation of gravity wave solution in the pressure gradient terms was used to conserves the basic principles of the dynamical part. A semi-lagrangian advectin scheme Faramawi [3] with fourth order accuracy has been used to increase the stability of the computation. It uses full physical parameterization package as a detail representation of radiation components and surface physics-soil hydrology processes. A comprehensive scheme for the planetary boundary layer with increase the number of layer under 1500 m to 6 levels has been used to improve the forecasting of the surface temperature and capture well all process occurring in the PBL layer. In addition to the cumulus scheme, a split cloud model with complicated microphysics was added to improve the simulation of the precipitation.

The Egypt-ETA has been used routinely in operation to give forecast up to 5 days. The results are very encouraging. In this paper, a dust module was under developing at Cairo NWP center to forecast and monitor the dust and sand storm. Since, in regions with high soil erosion, dust behaves as a pollutant that significantly reduces the air quality, in these areas ambient dust concentrations during dust storms may significantly exceed international standards for allowable concentrations Nickling and Gillies, [9], and therefore cause health problems such as allergy, respiratory diseases and eye infections, recently cases of life loose and property damages during extreme dust storm events were recorded in Sudan on May1996 and Egypt on May 1997 with dust load higher than $8g/m^2$ over the area of Cairo Nickovic,S.,: [10].

Substantial impacts of dust on climate and environment have increased needs to better understand and eventually predict the atmospheric dust cycle. Following such interest, an equation for sand concentration was added to the hydrostatic primitive Egypt – Eta model.

Two cases with very remarkable sandstorms were described and investigated through this study 14/03/1998 and 12/05/2001 and the model outputs for 72 hour were validated and verified by three manners to compensate the absence of actual data for sand load in our country by comparing it with the following factors:-

1) Actual data as (satellite images for aerosol index and visibility)

2) Aerodynamical parameters which are the main factors effecting on dust emission as (friction velocity - wind speed - vertical motion).

3) Synoptic situation, which associated with sand storm events.

1. Model description:

The model is based on the hydrostatic primitive equations, using a generalized vertical coordinate, η which follow the orographic structure (Simmons, A.J. and Burridge 1981). In the hybrid system a linear relation between η and the atmospheric pressure P defined as follow;

$$P(\eta) = A(\eta) + B(\eta) * P$$

Where, $A(\eta) = P_o\eta$, $B(\eta) = 0$ for $0 \le \eta \le \eta_T$

$$A(\eta) = \frac{P_o P_T}{P_o - P_T}(1-\eta) \quad , B(\eta) = \frac{P_o\eta - P_T}{P_o - P_T} \quad , \eta_T \le \eta \le 1$$

$$P_o = 1000hps \quad , P_T = 100hps$$

The forecasting equation in vertical coordinate $\eta(p, p_s)$ where $\eta(0, P_s) = 0$ and $\eta(P_s, P_s) = 1$.

The equations for the wind components are: -

$$\frac{du}{dt} + \eta\frac{\partial u}{\partial \eta} = -\frac{1}{a\cos\varphi}[\frac{\partial \phi}{\partial \lambda} + RT_u\frac{\partial \ln P}{\partial \lambda}] + fv + F_u \qquad (1.1)$$

$$\frac{dv}{dt} + \eta\frac{\partial v}{\partial \eta} = -\frac{1}{a}[\frac{\partial \phi}{\partial \varphi} + RT_V\frac{\partial \ln P}{\partial \Phi}] - fu + F_V \qquad (1.2)$$

Equation of thermodynamic;

$$\frac{dT}{dt} + \eta\frac{\partial T}{\partial \eta} = \frac{w\alpha}{C_P} + \frac{Q}{C_P} + F_T \qquad (1.3)$$

Equation of continuity;

$$\frac{\partial}{\partial \eta}(\frac{\partial P}{\partial t}) + \frac{1}{a\cos\varphi}\frac{\partial}{\partial \lambda}(u\frac{\partial P}{\partial \eta}) + \frac{1}{a}\frac{\partial}{\partial \varphi}(v\Phi\frac{\partial P}{\partial \eta}) + \frac{\partial}{\partial \eta}(\eta\frac{\partial P}{\partial \eta}) = 0 \qquad (1.4)$$

Let $\eta^* = \eta\frac{\partial P}{\partial \eta}$

The quantities F_U, F_V and F_T represent source terms, and also include any diffusion required for computational purposes. The vertical boundary conditions are for $\eta = 0$ And $\eta = 1$.

Equation of the local change of the surface pressure P_s, and the vertical velocity η, by integrating (1.4) in the vertical from $\eta = 0$ to 1.0, taking into account the boundary conditions we get the surface pressure tendency equation,

$$\frac{\partial P_s}{\partial t} = -\int_0^1 \frac{1}{a\cos\varphi}\left\{\frac{\partial}{\partial \lambda}\left(u\frac{\partial P}{\partial \eta}\right) + \frac{\partial}{\partial \varphi}\left(v\cos\varphi\frac{\partial P}{\partial \eta}\right)\right\}d\eta \qquad (1.5)$$

Again integrating (1.4) from $\eta = 0$ to a certain level $\eta = \eta_K$. Results in the equation for the vertical velocity $\dot{\eta}$ is in the form,

$$\dot{\eta}|_{\eta_K} = \left(\eta \frac{\partial P}{\partial \eta}\right)_{\eta_K} = -\left(\frac{\partial P}{\partial P_S}\right)_{\eta_K}\left[\frac{\partial P_S}{\partial t}\right] - \frac{1}{a\cos\varphi}\int_0^{\eta_K}\left\{\frac{\partial}{\partial\lambda}\left(u\frac{\partial P}{\partial \eta}\right) + \frac{\partial}{\partial\varphi}\left(v\cos\varphi\frac{\partial P}{\partial \eta}\right)\right\}d\eta \quad (1.6)$$

Where P_S is the surface pressure.

The hydrostatic equation is; $\frac{\partial \phi}{\partial \eta} = -RT_V\frac{\partial \ln P}{\partial \eta}$; with $\phi|_{\eta=1} = \phi_S$

The virtual temperature T_V is defined as; $T_V = T\{1 + 0.608q\}$

Where q is the specific humidity (kg/kg)

The vertical velocity in the pressure system $\omega = dP/dt$ which needed in the energy term $\alpha\omega$ for the conversion of potential and kinetic energy. For level $\eta = \eta_K$

$$(\alpha\omega)_{\eta_K} = (RT)_{\eta_K}\left(\frac{\omega}{P}\right)_{\eta_K}$$

Differentiating $\omega = dP/dt$ and inserting equation (1.6), the above equation yields that;

$$\left(\frac{\omega}{P}\right)_{\eta_K} = \frac{1}{P_{\eta_K}}\left[\begin{array}{l} -\frac{1}{a\cos\varphi}\int_0^{\eta_K}\left\{\frac{\partial}{\partial\lambda}\left(u\frac{\partial P}{\partial\eta}\right) + \frac{\partial}{\partial\varphi}(v\cos\varphi)\frac{\partial P}{\partial\eta}\right\}d\eta + \\ \frac{1}{a\cos\varphi}\left(u\frac{\partial}{\partial\lambda}\ln P + v\cos\varphi\frac{\partial}{\partial\varphi}\ln P\right)_{\eta_K} \end{array}\right] \quad (1.7)$$

The specific humidity q and the specific cloud liquid water content q_{DW} equations; the specific total water content q_{DW} is defined as;

$$q_{DW} = q_D + q_W$$

$$\frac{\partial q_{DW}}{\partial t} = -\frac{1}{a\cos\varphi}\left(u\frac{\partial q_{DW}}{\partial\lambda} + v\cos\varphi\frac{\partial q_{DW}}{\partial\varphi}\right) + \dot{\eta}\frac{\partial q_{DW}}{\partial\eta} - g\left(\frac{\partial P}{\partial\eta}\right)^{-1}\frac{\partial \eta_q}{\partial\eta} + \left(\frac{\partial q_{DW}}{\partial t}\right)_{sub} + F_H^{q_{DW}} \quad (1.8)$$

Where $F_H^{q_{DW}}$ stands for the horizontal diffusion, η_q is the vertical turbulent flux and $(\partial q/\partial t)_{sub}$ is the local time derivative by the other subscale process.

1.1) the time integration scheme:

The variables distribute on the semi-staggered E grid. The variable u, v, T, and q are holds at levels η_K where k is the index of the vertical level, while η', P and h holds at the intermediate level. The model uses a split explicit integration scheme similar to that introduced by Gadd [5]. To integrate using split-explicit formulation, the primitive equations are divided into two subsystems:

One includes those terms, which describe the inertia gravity wave oscillation called "Adjustment part ". I.e. this part includes the forward scheme that is applied to the pressure gradient term along with the trapezoidal implicit scheme for the coriolis term and the backward scheme to the w term and the tendency equation of surface pressure Janjic[6]. The other part contains low frequency, quasi- geostrophic motion, for which nonlinearly is usually dominant in the advection terms together with the diffusion terms, and is known as the advectoin stage.

The two stages are followed by physical parameterization.Vertical advection of temperature, momentum, and turbulent kinetic energy (TKE) is calculated using centered differencing, while specific humidity uses an upstream differencing technique. All variables use a Eular-backward time integration scheme Matsuno [7]. Horizontal advection scheme is performed using Lagrangen scheme Faramawi [3].

1.2) the horizontal (Semi-Lagrange) advection Scheme:

The Eulerian advection scheme regards the evolution of the atmospheric parameters at fixed geographic grid points. Such a scheme is well suited for regular Cartesian grids. Its time step, however, is rather limited due to stability reasons. On the other side, the Lagrange advection scheme follows the motion of individual air parcels. Such a scheme allows a much larger time step than the Eulerian scheme; its disadvantage is that originally regularly distributed air parcels will, after some time, exhibit a completely irregular pattern in the spatial dimension. The idea of the semi-Lagrange scheme is to combine the advantages of either scheme, i.e. the regular resolution of the Eulerian and the larger stability of the Lagrange scheme. This can be achieved when a different set of air parcels is regarded in each time step. This set consists of those air parcels, which have reached the position of a regular Cartesian grid point at the end of the respective time step. The method can be best explained by means of a passive one-dimensional advection. The one-dimensional equation of advection for a passive scalar quantity F can be written as:

$$\frac{dF}{dt} = \frac{\partial F}{\partial t} + U(x,t)\frac{\partial F}{\partial x} = 0 \qquad (1.9)$$

This equation implies that F remains constant along the air parcel's trajectory. As F(x,t) is known at all grid points x_m for the times $t_n - \Delta t$ and t_n, F can be computed for these grid points for the time $t_n + \Delta t$ by integrating (4.1) along the approximated air parcel trajectory:

$$\frac{F(x_m, t_n + \Delta t) - F(x_m - 2\alpha_m, t_n - \Delta t)}{2\Delta t} \qquad (1.10)$$

Where α_m is the distance of the air parcel covers in the direction x within the time interval Δt. If α_m is known, then the F-value at the end of the trajectory x_m at the time $t_n + \Delta t$ is identical to its value at the starting point $x_m - 2\alpha_m$ at the time $t_n - \Delta t$. In order to solve (1.10) the distance α_m must be determined, and $F(x_m - 2\alpha_m, t_n - \Delta t)$ has to be computed from the F-values at the grid points x_m.

The distance α_m is derived iteratively by solving the equation;

$$\alpha_m = \Delta t U(x_m - \alpha_m, t_n) \qquad (1.11)$$

i.e.

$$\alpha_m^{(k+1)} = \Delta t U(x_m - \alpha_m^{(k)}, t_n) \qquad (1.12)$$

A linear interpolation of the wind field is of sufficient accuracy to compute U at the point's $x_m - \alpha_m^{(k)}$. As (1.12) quickly converges, one or two iterations suffice to reach satisfactory accuracy. A linear interpolation, however, is not satisfactory to compute the function F at the starting point, i.e. $F(x_m - 2\alpha_m, t_n - \Delta t)$. . Here a cubic interpolation scheme is applied which leads to a spatial finite difference error of fourth order with very little damping which smoothes the smallest resolved scales only.
The multiply upstream semi-Lagrangian advection scheme suitable for the horizontal advection terms on the E-grid has been used. Faramawi [3] designed and illustrated this scheme which has the following advantage:

-The maximum value of the amplification factor did not exceed the unity.
-The schemes are absolutely stable.
-The damping effect decreases with increasing wavelength.

To use this scheme operationally, the trajectory first determines by iteration procedure. It was found that two iterations are sufficient to correct the departure point position. 9-points interpolation scheme has been used to determine u & v components of the wind at the end of the trajectory. The advected property at the departure point was calculated using 13-point interpolators, which gives fourth order accuracy. On the lateral boundaries the 5-points interpolators was used. The choice of 5-points scheme on the outer lines is to reduce the small-scale wave's motion and prevent it from entering the interior of the integration domain.

2- Module of the atmospheric dust cycle

The dust module associated with the Egypt - Eta (EGETA) model consists of the following basic components

1- Emission of dust from the source areas
2- Horizontal and vertical transport, including turbulent mixing in the vertical
3- Wet and dry deposition

2.1- Dust emission

Dust continuity equation in general expressed as:

$$\frac{\partial C_k}{\partial t} = -u\frac{\partial C_k}{\partial x} - v\frac{\partial C_k}{\partial y} - (\omega - v_{gk})\frac{\partial C_k}{\partial z} - \nabla(k_h \nabla C_k) - \frac{\partial}{\partial z}(k_z \frac{\partial C_k}{\partial z}) + (\frac{\partial C_k}{\partial t})_{source} + (\frac{\partial C_k}{\partial t})_{sink} \quad (2.1)$$

This is the desert dust cycle and it is described by K EULER-type concentration equations here k is the number of considered particle size classes and as Tegan and Fung [13].
Under neutral stability conditions, the surface concentration can be expressed in terms of vertical surface flux as Nickling and Gillies, [8]

$$C_{sk} = const \quad \frac{F_{sk}^{eff}}{ku_*} \quad (2.2)$$

This should lead us to define the effective value of the flux at a source point (i,j)as

$$(F_{kl})_{eff}\ (i,j) = \delta_{kl}(i,j)\ f_l(i,j) \quad (2.3)$$

$$\delta_{kl}(i,j) = \alpha(i,j)\ \beta_k\ \gamma_k(i,j)$$

This is the factor that represents properties of desert soils and is called the dust productivity factor.

$\alpha(i,j)$ is the fraction of a grid point area covered by desert surface and it is calculated by:

α =area covered by desert /area of grid box

$$\alpha^{i,j} = \sum_{m=1}^{4} \Psi_m^{i,j} M_m^{i,j}$$

The summation is done over four nearest global grid points surrounding a model grid point (i,j), where Ψ_m is the bilinear interpolation-weighting factor. And M is depending on vegetation cover and to define geographical distribution of the vegetation, a subjective correspondence is established between the Olson World Ecosystems EPA, [2] having 59 classes at 10 min resolution, and the 13 SSIB vegetation types required by Eta/NCEP model. This data is mapped into the EGETA grid to define the desert points. Dust productive areas are distinguished from the others by the desert where mask M=1or no desert where mask M=0 calculated from vegetation types given in table (1).

Table (1)

Code number	Vegetation type
8	Desert, mostly bare stone, clay and sand
50	Sand desert, partly blowing dunes
51	Semi desert, desert scrub, sparse grass
52	Cool, cold shrub semi desert, steppe

Seven texture classes of Zobler [16] are distributed over the model grid points. In Table (2), the Zobler texture classes are corresponded to Cosby et al. (1984) soil types. The table also gives the matrix $\beta_{kl}^{i,j}$ which is the fraction of soil for a given particle size k and for a particular texture class representative for a grid point (i,j). Contribution to soil erosion is specified according to particle size features of clay, small silt, large silt and sand. Fractions of these four classes are estimated from the clay/sand/silt triangle Tegan and Fung [13].

Table (2) relative contributions of clay /sand/silt for considered Seven texture /soil categories

L	Zobler Texture classes	Cosby et al. Soil types	β_{kl} (fractions) Clay	silt	sand
1	Coarse	Loamy Sand	0.12	.08	0.8
2	Medium	Silty Clay Loam	.34	.56	0.1
3	Fine	Clay	.45	.3	.25
4	Coarse-Medium	Sandy Loam	.12	.18	0.7
5	Coarse-Fine	Sandy Clay	.40	.1	0.5
6	Medium-Fine	Clay Loam	.34	.36	0.3
7	Coarse-Medium-Fine	Sandy Clay Loam	.22	.18	0.6

The ratio between the mass available for uplift and the total mass (γ_k) is also summarized in table (3)

Table (3) features of dust particles for typical size classes

Type K=1,2,3,4	Size distribution	Particle radius R_k(um)	Particle density ρ_k (g cm^{-3})	γ_k
Clay	dM/d log r=const	0.5-1 (.73)	2.5	0.08
Small silt	dM/d r =const	1-10 (6.1)	2.65	1.00
Large silt	dM/d r =const	10-25 (18)	2.65	1.00
Sand	dM/d r =const	25-50 (38)	2.65	0.12
Sand	dM/d r =const	25-50 (38)	2.65	0.12

Tegen and Fung [13] used functional form for vertical dust flux

$$f_s^{i,j} = const(u_*^{i,j})^3 [1-(\frac{u_{*t}^{i,j}}{u_*^{i,j}})] \qquad (2.4)$$

u_{*t} is the threshold friction velocity bellow which dust injection into the atmosphere is ceased and its value depends on a soil texture type I(I , j) .

$$u_{*tk} = u_{*tkd}\sqrt{1+1.21(w-w^{\circ})^{0.68}} \qquad (2.5)$$

u_{*tkd} threshold friction velocity for dry soil defined by Bagnold [1]

$$u_{*tkd} = A_k\sqrt{2gR_k(\rho_{pk}-\rho_a)\div\rho_a} \qquad (2.6)$$

We specify A_k ={1,.7,.4,.25} for the considered four particle sizes White, [14]. W is the ground wetness predicted by the atmospheric model, and w° is the saturated ground wetness.

Fecan et al, made an empirical relationship between w° and soil clay content has been established to be a second order polynomial function of clay fraction in soil

w° =0.0014(%clay)^2 + 0.17(%clay)

2.2 - dust sink

Particulate is ultimately removed from the atmosphere by one of two mechanisms: -

a) Dry deposition

The dry deposition process is represented in terms of a deposition velocity v_d thus, the deposition velocity is best viewed as a proportionality constant between vertical downward flux [v_d c (x,y,z,t)] and concentration of species.

Where c is the concentration predicted by the atmospheric diffusion equation.

Since there is a physical similarity of mass/heat/momentum exchange over surfaces Segal, [11] we can apply the same viscous sub-layer model to the dust deposition, as well. Following Janjic [6], the dust sink term in the concentration equation is represented by

$$\left(\frac{\partial c_k}{\partial t}\right)_{ddep} = -\frac{flux}{\Delta z} = -\frac{v_d c}{\Delta z} \qquad (2.7)$$

Where Δz is the depth of the lowest model layer.

The dry deposition process can be viewed conceptually by analogy to electrical or heat flow through a series of resistances. The transfer of material from the atmosphere to the surface takes place through three resistances, the aerodynamic resistance, the surface layer resistance, and the transfer resistance these resistances are denoted R_a, R_s and R_t and they have units of sec cm^{-1} their relation to v_d is

$$V_d=(R_a+R_s+R_t)^{-1} \quad (2.8)$$

Where, R_a is the aerodynamic resistance , R_s is the surface layer resistance, and R_t is the transfer resistance.

The aerodynamic resistance R_a accounts for the turbulent diffusion of material from the free atmosphere to the surface laminar sub layer, thus R_a depends on the usual meteorological parameters, such as wind speed, atmospheric stability and surface roughness and is given by

$$R_a(z, z_0) = \frac{(\ln(z / z_0))^2}{k^2 \bar{u}(z)}$$

The surface layer resistance R_s depends on parameters characterizing diffusion across a laminar sub layer and thus on molecular rather than turbulent properties.

$$R_s = (sc^{-2/3} + 10^{-3/st})^{-1} u_*^{-1}$$

The transfer resistance depends on the physico-chemical interaction between the material and the surface.

For dry deposition of particles that transfer resistance R_t is absent, since once the particle encounters the surface it is considered to have deposited. Also if the particle has appreciable settling velocity v_s, that settling velocity contributes to the deposition rate.

$$V_d=(R_a+R_s+R_aR_sV_s)^{-1}+V_s \quad (2.9)$$

Where $V_s = \frac{(r_p)^2}{18\mu}(\rho_p - \rho)g$ (2.10)

μ is the air viscosity Sc Schimdt number St Stokes number

b) Wet deposition

Absorption into droplets followed by droplet removal by precipitation.

The rate of dust scavenged by precipitation is calculated as

$$\frac{\partial c}{\partial t} = -\frac{\partial}{\partial z}(\Phi c \frac{\partial p}{\partial t}) \quad (2.11)$$

Precipitation rate is $\frac{\partial p}{\partial t}$ and Φ is washout parameter (500000).

3. Validation of Dust model

Validation (1) is based on the comparing of the location of dust forecasted by the model with the cold front and satellite image for aerosol index.

The model had a qualified job in predicting dust load either by development or movement up to 3-day forecast using the analysis of 14 March 1998(1200 UT) as initial data. The forecasted dust over Egypt was accurate during the forecast period with southerly wind and extremely associated with the cold front fig (1a, 1b, 1c). Also the comparing of the location of the dust load forecasted by the model with Images for satellite for aerosol index, which is indicator to the dust load in the atmosphere. At 14/3/1998 the maximum aerosol index centered over Libya fig. (2a) move northeast to center at 15/3/1998 over Egypt fig (2b)

and continue to cover only the east region and south of Egypt in the third day fig. (2c) as the out put of the model.

Dust load (g/m^2) shaded and temperature 850 mb (contour)	Earth Probe TOMS Aerosol index
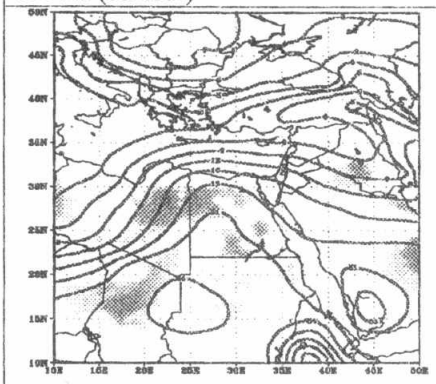	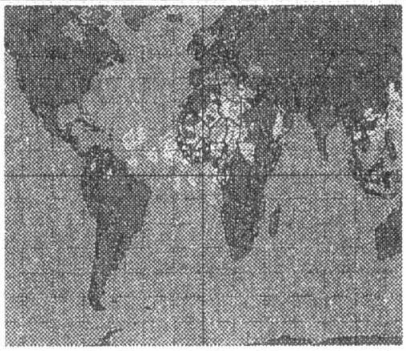
Fig (1a) +48 hour forecast	Fig (2a) 14/3/1998
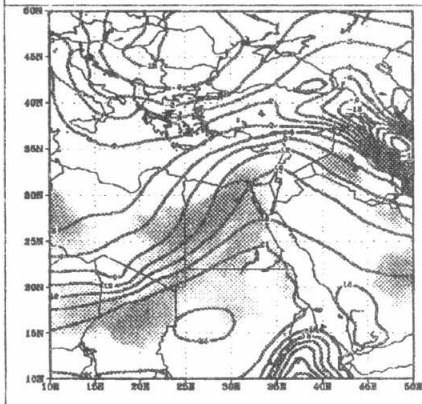 Fig	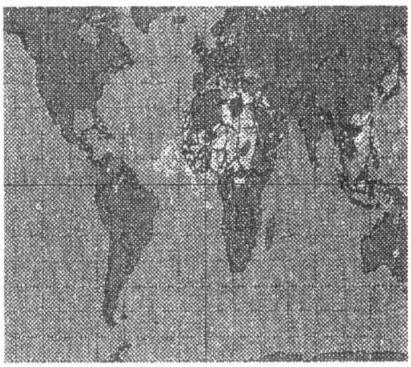
(1b) +72 hour forecast	Fig (2b) 15/3/1998
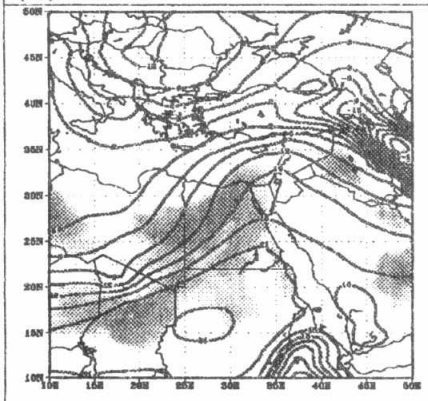	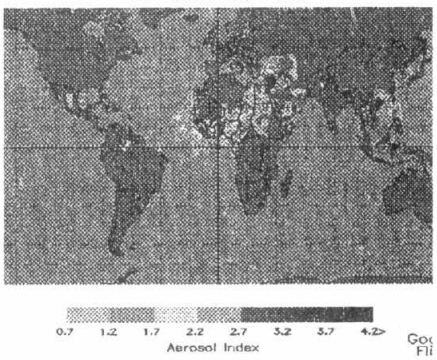
Fig (1c) +72 hour forecast	Fig (2c) 14/3/1998

Validation (2) is based on the comparing of the location of dust load forecasted by the model with some of meteorological parameter which are the main factors effecting on dust emission as (friction velocity - wind speed - vertical motion) over two stations Cairo (inland station) and Matruh (Coastal station).
As shown in fig (3 & 7) it is obvious proven that there is a direct proportionality between dust load in the atmosphere with the wind speed also wind speed reach to its maximum value before dust reaches its maximum value since wind speed is one from the factors which affect dust emission and dust particles usually have a small terminal velocity and therefore they tend to remain suspended in air for along time before deposition.

model outputs with surface observation will be presented for two stations, coastal one (Matruh) and inland one (Cairo) as shown in fig (5 & 8). In the two stations show that the dust emission starts to increase sharply when u_* reach over 0.5(m/s) but u_* is effective only in releasing sand from the soil not in the upward motion mechanism.

Also as shown in figures (4 & 6) down ward motion needed to makes excitation for dust to liberated from the soil and then up ward motion will be the main factor to lift the dust to different heights according to it's intensity and the weight of the parcel and this shown in the three stations before the dust storm downward motion occur and during the dust storm upward motion occur.

Fig. (3) Variation of Wind speed and dust load (g/m^2) with time over Cairo

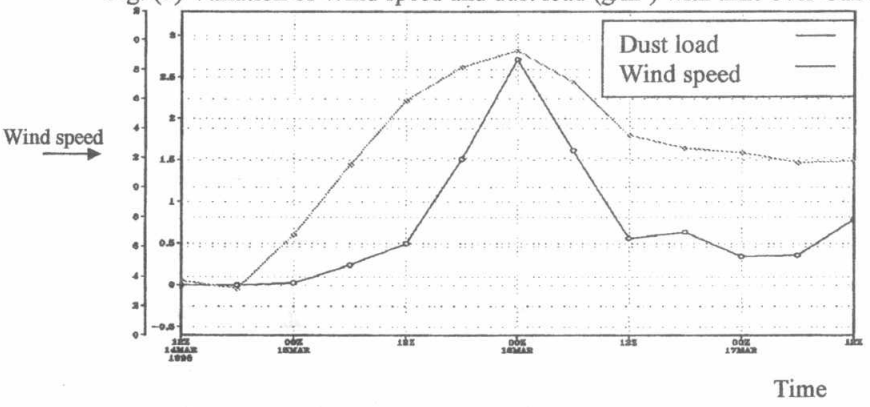

Fig. (4) Variation of Vertical motion and dust load (g/m^2) with time over Cairo

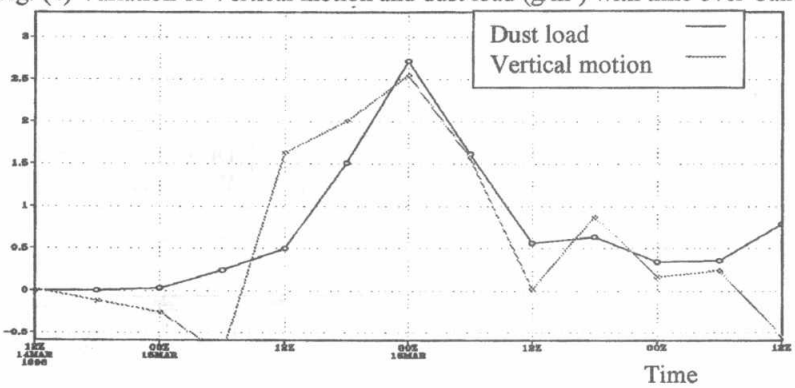

Fig. (5) Variation of Friction velocity (u_*) and dust load (g/m^2) with time over Cairo

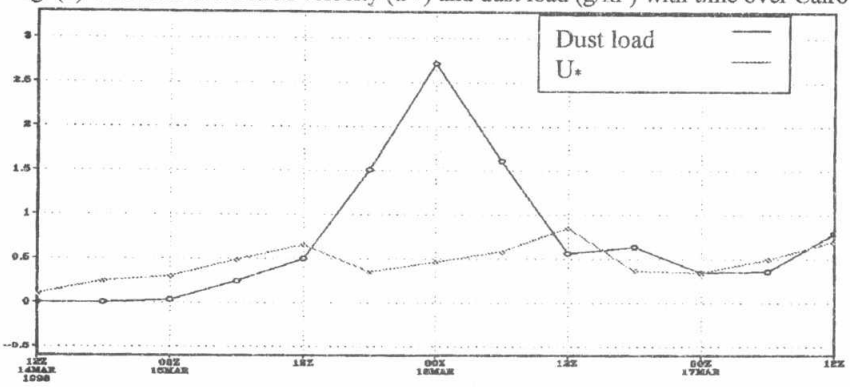

Time

Fig. (6) Variation of Vertical motion *10 and dust load with time at Matruh

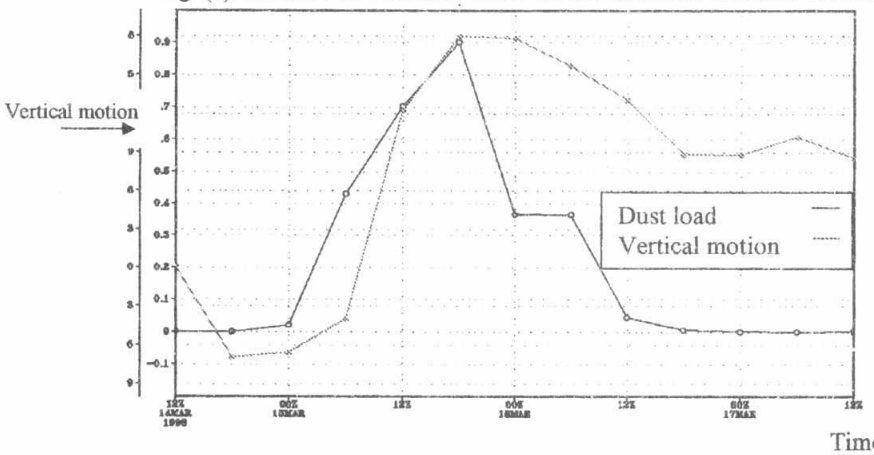

Time

Fig. (7) Variation of wind speed and dust load (g/m^2) with time over Matruh

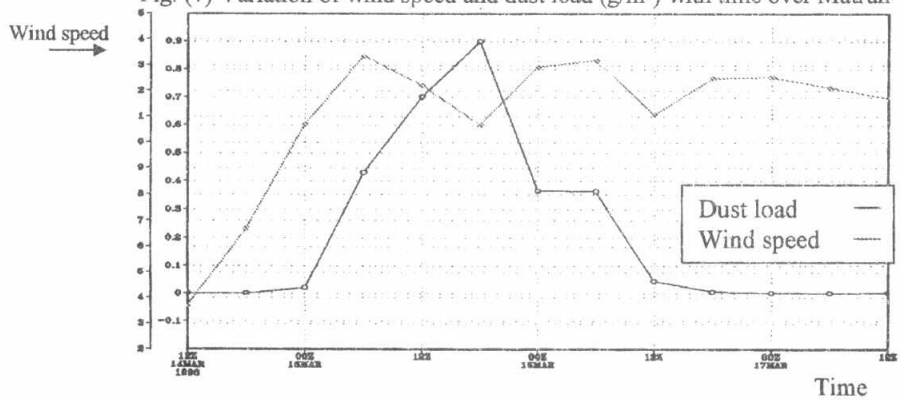

Time

Fig. (8) Variation of Friction velocity (U_*) and dust load (g/m^2) with time over Matruh

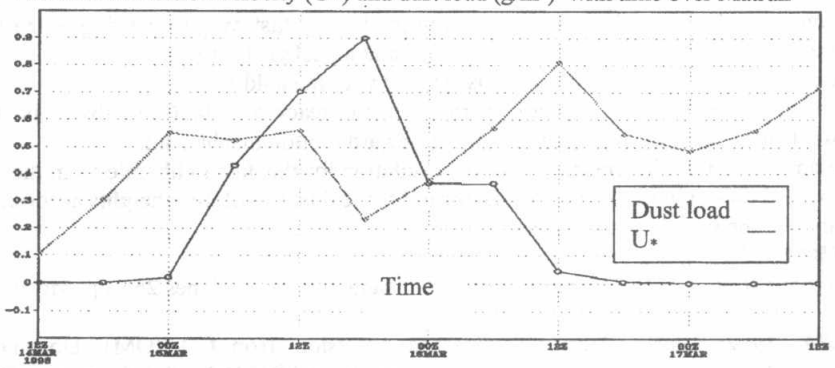

Case of 12/05/2001 (initial data 11/05/2001 1200utc)

As shown in fig (9a & 9b) there is complete convenience between visibility deterioration and increasing of dust load in the two stations moreover it is observed that as dust load greeter than 0.9 g/m^2 as visibility decrease to less than 200 m.

Fig (9a) visibility and dust load*10 over Cairo at the period of forecast

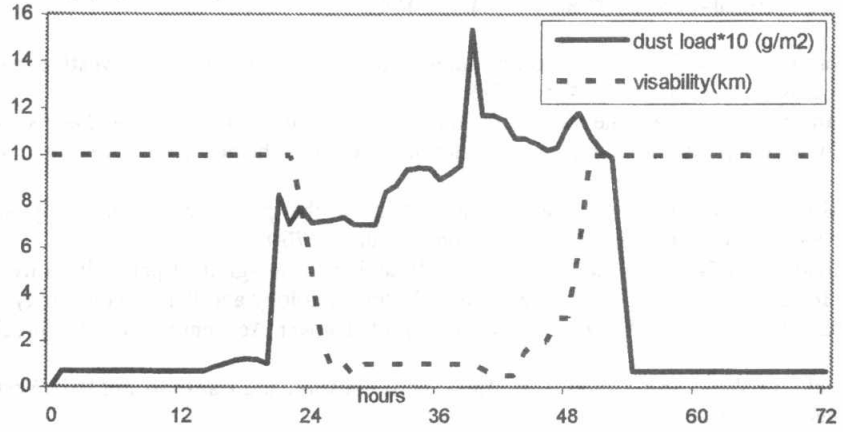

Fig (9b)) visibility and dust load*10 over Alex at the period of forecast

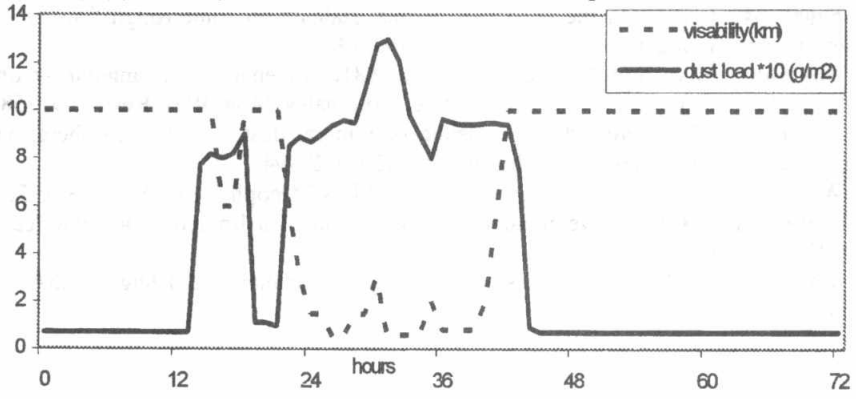

Conclusion

1-The model had an excellent performance in predicting dust over Egypt during the forecast period when compared with the satellite images and actual visibility.

2- The dust storm events are extremely associated with the cold front.

3-The dust emission start to increase sharply when u_* reach over 0.5(m/s) also u_* is effective only in releasing sand from the soil not in the upward motion mechanism.

4- The down ward motion needed to makes excitation for the dust to liberate from the soil and then up ward motion will be the main factor to lift the dust to different heights according to its intensity and the weight of the parcel.

REFERENCES

1:- Bagnold,R.A., 1941: The physics of blown sand and desert dunes,265 pp.,Morrow, New York,.

2:- EPA, 1992: Global Ecosystem Database, Version 1(on CD-ROM). Documentation Manual, EPA global change Research program-NOAA/NGDC Global change Database program, USDC, Clorado,.

3:- Faramawi. U, A, 1996: An advection scheme for primitive equations N.W.P. mode. Msc. Thesis, pp 72.

4:- Fecan, F.,B.Marticorena,and G.Bergametti, 1999: Parameterization Of the increase of the Aeolian erosion threshold wind friction velocity due to soil moisture for arid and semi – arid areas. Annales Geophysicae, 17,194-157,1999.

5:- Gadd, A. J., 1978: A split explicit integration scheme for numerical weather prediction. Quart. J. Roy. Meteor. Soc.104, 569-582.

6:- Janjic, Z.L., 1994: The step-mountain Eta Coordinate Model: Further Developments of the Convection, Viscous Sublayer and Turbulence closer schemes, Mon. Wea.Rev., 122,927-945,

7:- Matsuno, T., 1966: Numerical integration of the primitive equations by simulated backward difference method. J. Meteor. Soc., Japan, 44, 76-84.

8:- Nickling W.G. and Gillies J.A., 1989: Emission of fine-grained particulates from desert soils. In: Leinen M. and Sarnthein M. (eds), Paleoclimatology and Paleometeorology: Modern and past patterns of global atmospheric transport, Kluwer Academic Publ., Dordrecht, 133-165.

9:- Nickling W.G. and Gillies J.A., 1993: Dust emission and transport in Mali, West Africa, Sedimentology,40,859-868.

10:-Nickovic,S.,: 2001, A model for prediction of desert dust cycle in the atmosphere, J. Geophys. Res. 106, 18113-18130.

11:- Segal, M., 1990: On the impact of thermal stability on some rough flow effects over mobile surfaces, Boundary-Layer Meteor.,,52 , 193-198.

12:- Simmons, A. J. and Burridge, D., M. 1981: An energy and angular –momentum conserving finite-difference scheme and hybrid coordinates. Mon. Wea. Rev., 109, 758-766.

13:- Tegen,I., and I.Fung, 1994: Modeling of mineral dust in the atmosphere: sources , transported optical thickness,J.Geophys.Res.,99,22987-22994,.

14:- White,B.R., 1979: Soil transport by winds in Mars,J.Geophys.Res.,84,4643-4651.

15:-Yousef. A. S. 1988: Development and application of a limited area numerical model. Ph.D. Thesis. 170pp.

16:- Zobler, L., 1986: A world soil file for global climate modeling. NASA . Techn. Memo.87802.